Dennis Wiedemann*, Suliman Nakhal, Anatoliy Senyshyn, Thomas Bredow, and Martin Lerch

The High-Temperature Transformation from 1T- to 3R-Li$_x$TiS$_2$ ($x = 0.7, 0.9$) as Observed *in situ* with Neutron Powder Diffraction

Abstract: Layered titanium disulfide is used as lithium-ion intercalating electrode material in batteries. The room-temperature stable trigonal 1T polymorphs of the intercalates Li$_x$TiS$_2$ ($x \leq 1$) are widely-investigated. However, the rombohedral 3R polymorphs, being stable at higher temperatures for large x, are less well known. In this study, we report on the synthesis of phase-pure 1T-Li$_x$TiS$_2$ ($x = 0.7, 0.9$) and its transformation to the 3R phase between 673 and 873 K as monitored using high-temperature neutron powder diffractometry. For the 3R polymorph, full Rietveld refinements show lithium ions to be statistically distributed over octahedral voids at the fractional coordinates 0, 0, $^1/_2$, exclusively. The comparison of Madelung energies with results of periodic quantum-chemical calculations reveals that the evolution of lattice parameters and the room-temperature stability of the 1T phase are not governed by electrostatics, but by correlation and polarization. The insights gained do not only elucidate the structure of 3R-Li$_x$TiS$_2$, but also help to understand and control polymorphism in layered transition-metal sulfides.

Keywords: Lithium-Ion Conductors, Lithium Transition-Metal Sulfides, Layered Structures, Phase Transformation, Thermal Expansion.

*Corresponding author: Dennis Wiedemann, Institut für Chemie, Technische Universität Berlin, Straße des 17. Juni 135, 10623 Berlin, Germany, e-mail: dennis.wiedemann@chem.tu-berlin.de
Suliman Nakhal, Martin Lerch: Institut für Chemie, Technische Universität Berlin, Straße des 17. Juni 135, 10623 Berlin, Germany
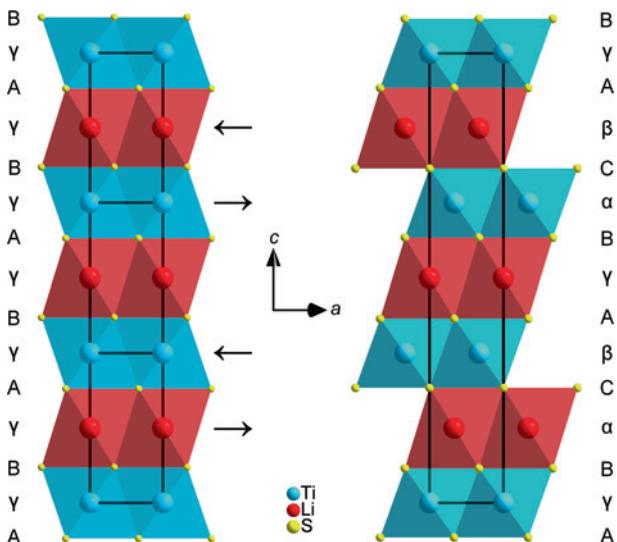**Anatoliy Senyshyn:** FRM II, Technische Universität München, Lichtenbergstraße 1, 85747 Garching b. München, Germany
Thomas Bredow: Mulliken Center for Theoretical Chemistry, Universität Bonn, Beringstraße 4, 53115 Bonn, Germany

1 Introduction

Being able to host small species like ammonia, water, sodium, and lithium ions, layered titanium disulfide is a well-known electrode material for lithium batteries [1–3]. Lithium ions easily intercalate into its van-der-Waals (vdW) gaps under electrochemical or chemical treatment resulting in (lithium-deficient) single-phase lithium titanium disulfides Li_xTiS_2 ($x \leq 1$). If chemical lithiation is conducted slowly, an ordered $1 \times 1 \times 3$ superlattice structure is observed for $x = 0.33$. For all other lithium contents or reaction protocols, a statistical distribution of the lithium ions is found [4].

So far, two layered polymorphs of Li_xTiS_2, differing in their stacking sequences, have been observed: the 1T and the 3R phase (see Figure 1). Trigonal 1T-LiTiS$_2$ (space group: $P\bar{3}m1$) constitutes a structure type of its own. Alternating layers (M = Ti, Li) of edge-sharing MS$_6$ octahedra are linked via common faces, the anion stacking sequence being AB. Hypothetically shifting every second/third metal layer by $^1/_3$ along [100]/[$\bar{1}$00] with sulfide ions following, rhombohedral 3R-LiTiS$_2$ (NaCrS$_2$ type, space group: $R\bar{3}m$) is acquired. In this second known polymorph, the coordination octahedra of different cation types no longer share faces, but edges instead. The anion stacking sequence ABC with alternating lithium- and titanium-ion layers results in a roughly tripled lattice parameter c compared to

Figure 1: Crystal structures of 1T- (left) and 3R-LiTiS$_2$ (right). View along [010], unit-cell edges in black, stacking sequences at the margins, arrows indicating the hypothetical movement during the transformation 1T → 3R.

the 1T phase [5]. Besides these layered polymorphs, defect-spinel type c-LiTiS$_2$ is accessible from c-LiTi$_2$ (Ti$_2$C type, space group: $Fd\bar{3}m$) [6]. The structure of the latter can be rationalized as deriving from that of 1T-LiTi$_2$ (CdI$_2$ type) by transferring one fourth of the titanium ions to the vdW gap between sulfide layers. Further details concerning this phase are well beyond the scope of this publication.

Being the thermodynamically most stable ones at room temperature, the 1T-Li$_x$TiS$_2$ polymorphs are most widely-investigated. Their crystal structure with respect to the lithium-ion positions has been unambiguously elucidated by neutron powder diffractometry for x = 0.12, 0.33, 0.67, and 1. A formerly discussed occupation of tetrahedral voids has been ruled out [7]. Also, the influence of x on the lattice parameters has been extensively and comparatively studied with materials of different origins [8]. Although Colbow et al. have described 3R-Li$_x$TiS$_2$ for x > 0.4 as early as in 1989 [5], it was not until 2013 that we have been able to report on the crystal structure of 3R-LiTiS$_2$ and compare its stabilities to those of other (partly hypothetical) polymorphs. However, as X-ray diffractometry was employed, experimental verification of the assumed lithium-ion positions is still lacking [9]. Very recently, a comprehensive study comprising a phase diagram (x vs. T) for the system 1T-/3R-Li$_x$TiS$_2$ has been published [10].

In this work, we present the results of a full Rietveld refinement using neutron powder diffractograms of 1T-/3R-Li$_x$TiS$_2$ (x = 0.7, 0.9) at 297, 473, 673, 873, and 973 K to shed more light on the high-temperature behavior and the structural relations between the two polymorphs.

2 Experimental

2.1 Synthesis

Polycrystalline 1T-TiS$_2$ was prepared by direct synthesis from titanium and sulfur (Fa. Merck) in an evacuated silica ampoule. The ampoule was first held at 400 °C for 10 d to achieve complete reaction of the elemental sulfur, then at 700 °C for further 7 d. Subsequent chemical lithiation was carried out to yield materials of the compositions Li$_x$TiS$_2$ (x = 0.7, 0.9). For this purpose, a suspension of 1T-TiS$_2$ in a solution of nBuLi in hexane (c = 2.5 mol · dm^{-3}) was stirred under dry dinitrogen at r.t. for 7 d. The solvent was evaporated in vacuo and the remaining solid kept in a compartment dryer at 100 °C for two days. Afterwards, it was freed of residual moisture by drying in vacuo at 150 °C before being transferred into a silica ampoule. After evacuation, the latter was placed in an oven to anneal the

intercalation compound at 500 °C for 10 d. In order to prevent any decomposition or reaction with moisture, the sample was then kept and handled under dry argon.

At all stages, phase purity was checked by powder X-ray diffraction using a "PANalytical X'Pert PRO MPD" diffractometer in Bragg–Brentano (θ–θ) geometry equipped with Cu-K_α source and a "PIXcel" detector. Rietveld refinements were carried with the FullProf 2006 suite using pseudo-Voigt profile functions [11]. The absence of oxygen compounds was confirmed by analysis with a "Leco EF-TC 300" N_2/O_2 analyzer (hot-gas extraction). The absence of silicon compounds was ensured by X-ray fluorescence analysis using a "PANalytical Axios PW4400/24" spectrometer with a rhodium tube and a wavelength dispersive detector. Lithium contents were confirmed after microwave digestion with nitric acid using an optical-emission spectrometer "Varian ICP-OES 715" equipped with a Sturman-Masters spray chamber.

2.2 Neutron powder diffractometry

Diffraction experiments were conducted at the neutron source FRM II (MLZ, Garching b. München) using the high-resolution powder diffractometer SPODI with Ge(551)-monochromated neutrons (λ = 154.829 pm) in Debye–Scherrer geometry [12]. The powder samples were compacted in a niobium cylinder (d = 8 mm, h = 15 mm) and mounted in a vacuum high-temperature furnace. Measurements were carried with an exposure time of 5 h each. Data were recorded with an array of 80 position-sensitive ^{3}He tubes ($2\theta_{max}$ = 160°, effective height: 300 mm) and reduced using a variable-height algorithm as implemented in the in-house parser [12], yielding a final range of $0.95° \leq 2\theta \leq 151.90°$ with $\Delta(2\theta) = 0.05°$.

As a starting point for refinement of the 3R-type phases, a known model for $NaCrS_2$ from the Inorganic Crystal Structure Database (ICSD) was imported and adjusted to reflect the actual cell parameters and contents [13]. Models were then refined with Jana2006 against 2θ data analytically corrected for absorption (cylindrical sample) using the full-matrix least-squares algorithm [14].

Regions containing the very strong reflections of the niobium container or weak non-overlapping side-phase reflections were excluded from the refinement. (The latter were caused by a small amount of TiO_2 [rutile type] in $Li_{0.7}TiS_2$ [$w < 0.01$; at ca. 36.1°, 41.3°, 69.1°, and 77.7°] and by a small amount of Li_xTiO_2 [NaCl type] in $Li_{0.9}TiS_2$ [$w \ll 0.05$; at ca. 31.2°, 37.5°, 43.1°, 76.0°, and 106.2°] that had not occurred before sample handling in the neutron-source facility and are probably due to reaction with traces of dioxygen or moisture.) The background was defined manually with 35–53 points that were interpolated using ten Legendre polynomials with refined coefficients. Reflection profiles were fitted with

a pseudo-Voigt function following the Thompson–Cox–Hastings approach [15]. Asymmetry was corrected for using the two-term Bérar–Baldinozzi method [16]. The approach of March and Dollase was employed to model a preferred orientation in (001) [17, 18]. All atoms were refined with anisotropic atomic displacement parameters. Structure pictures were prepared using Diamond [19], diagrams were plotted with OriginPro [20].

Further details of the crystal-structure investigations may be obtained from *Fachinformationszentrum Karlsruhe*, 76344 Eggenstein-Leopoldshafen, Germany (fax: +49 7247 808-666; e-mail: crysdata@fiz-karlsruhe.de, http://www.fiz-karlsruhe.de/request_for_deposited_data.html) on quoting the deposition numbers CSD-428812 to CSD-428821.

2.3 Computational methods

Madelung parts of the lattice energies were calculated using the Madel facility of Vesta [21]. The lattice parameters and atomic positions were set to the experimental values (Tables 1, 4, and 5); lithium occupancies were set to match the formulae. According to the Mulliken net charges obtained in the quantum-chemical calculations (see below), the ionic charges were reduced by one half for the calculation of Madelung energies. The point-charge model applied here does not account for polarization effects and is only a crude approximation of the electrostatic potential. However, in a previous study of Zr_2ON_2 [22], it was shown that relative stabilities of anion distributions obtained with Maple [23] are in semi-quantitative agreement with quantum-chemical results.

For density-functional theory (DFT) calculations, the functional PBE [24, 25] as implemented in the crystalline-orbital program Crystal09 [26] was applied. Since the quality of the wavefunction and therefore of the energies critically depends on the basis sets (BS), we employed three BS of increasing quality. **A** denotes the combination of (864-11G31d (Ti) [27], 7-11G1d (Li) [28], and 86-311G1d (S) [27]; in **B**, the sulfur BS was replaced by cc-pVTZ [29]; in **C**, sulfur and lithium BS are cc-pVTZ [30], and the titanium BS is a truncated def2-QZVPPD [31] without diffuse functions. In particular, the latter BS can be considered as close to the basis set limit. Calculated energies refer to unrestricted Kohn-Sham calculations without explicit specifications of the spin state (SPINLOCK). Standard integral thresholds and $6 \times 6 \times 6$ Monkhorst-Pack grids were used. $Li_{0.67}TiS_2$ was modeled using a $(-1 -2\,0,\, 2\,1\,0,\, 0\,0\,1)$ supercell and removing one lithium ion. Energies were normalized to one titanium ion. Experimental lattice parameters and atom positions from this work were taken and kept fixed. In one case, it was checked that full optimization did not alter the relative stability by more than $1.8\ kJ \cdot mol^{-1}$.
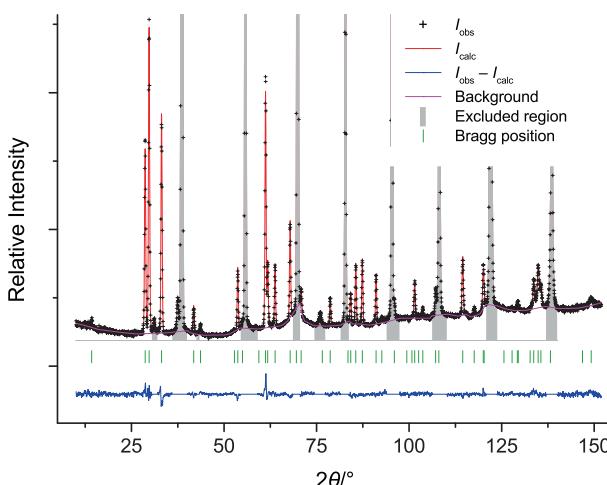
3 Results and discussion

3.1 Refinement

As the samples had to be measured in an inert beaten niobium cylinder, the resulting strong reflections of the container had to be cut out of the diffractograms for handling with Jana2006. The remaining background proved to be complex, but did not prohibit high-quality refinement (see Figure 2). The fit of the model is somewhat better for the 3R phases and for $x = 0.9$, probably due to a less pronounced preferred orientation. Details are summarized in Table 1.

3.2 Phase transformation

Between 673 and 873 K, the 1T transform into 3R phases for both lithium contents (see Figure 3). This finding is in accordance with the phase diagram published by Zhang et al. [10]: Although data points for $x = 0.7$ and 0.9 are not included in it, transformation temperatures of ca. 840 and 800 K, respectively, may be interpolated. To check the reversibility exemplarily, the sample of $Li_{0.9}TiS_2$ was measured again at room temperature after having been heated to 973 K. No differences between the diffractograms of the pristine and cooled material were found.

The 1T and 3R phase derive from the cubic and hexagonal close-packed lattice, respectively; no direct group-subgroup relationship exists between them. Be-
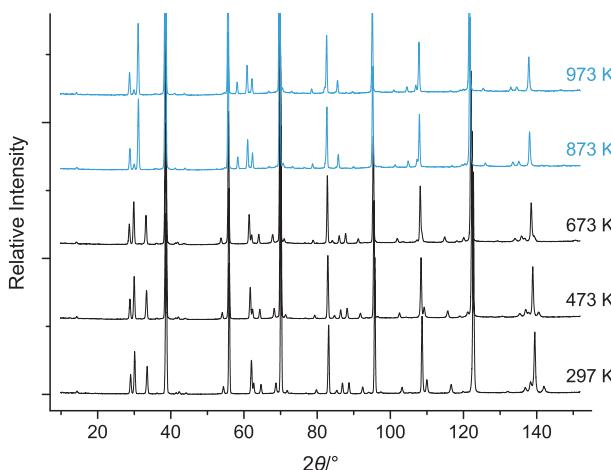

Figure 2: Exemplary neutron diffractogram of $1T\text{-}Li_{0.9}TiS_2$ at 673 K with fit and background data.

Table 1: Details of the Rietveld refinements.

	1T-Li$_{0.7}$TiS$_2$			3R-Li$_{0.7}$TiS$_2$		1T-Li$_{0.9}$TiS$_2$			3R-Li$_{0.9}$TiS$_2$	
T/K	297	473	673	873	973	297	473	673	873	973
CSD no.	428812	428813	428814	428815	428816	428817	428818	428819	428820	428821
Space group	$P\bar{3}m1$	$P\bar{3}m1$	$P\bar{3}m1$	$R\bar{3}m$	$R\bar{3}m$	$P\bar{3}m1$	$P\bar{3}m1$	$P\bar{3}m1$	$R\bar{3}m$	$R\bar{3}m$
Crystal system	trigonal	trigonal	trigonal	trigonal	trigonal	trigonal	trigonal	trigonal	trigonal	trigonal
M_r	116.9	116.9	116.9	116.9	116.9	118.2	118.2	118.2	118.2	118.2
a/pm	343.760(7)	345.531(7)	346.353(11)	350.061(6)	349.659(7)	345.426(5)	346.751(6)	348.117(6)	352.143(8)	353.131(8)
c/pm	617.866(19)	622.13(2)	625.10(3)	1865.83(5)	1865.29(7)	619.103(13)	622.062(12)	624.917(14)	1855.91(6)	1860.89(6)
$V/10^6\,\mathrm{pm}^3$	63.232(3)	64.326(3)	64.940(6)	198.011(10)	197.500(13)	63.9740(19)	64.774(2)	65.585(2)	199.308(13)	200.967(13)
Z	1	1	1	3	3	1	1	1	3	3
$\varrho_{\mathrm{calc}}/\mathrm{g}\cdot\mathrm{cm}^{-3}$	3.0688	3.0166	2.9881	2.9400	2.9476	3.0693	3.0314	2.9939	2.9555	2.9311
wR_p [1]	0.0452	0.0396	0.0367	0.0273	0.0322	0.0345	0.0300	0.0288	0.0264	0.0261
wR_{exp} [1]	0.0345	0.0236	0.0199	0.0225	0.0312	0.0235	0.0224	0.0217	0.0214	0.0213
R_B [$I>3\sigma(I)$]	0.0424	0.0552	0.0495	0.0283	0.0356	0.0378	0.0425	0.0479	0.0230	0.0340
S [all refl.]	1.31	1.68	1.84	1.22	1.03	1.47	1.34	1.33	1.23	1.22
R_F [all refl.]	0.0303	0.0345	0.0313	0.0446	0.0451	0.0258	0.0262	0.0350	0.0282	0.0330
r^2 [2]	1.069(4)	1.087(4)	1.082(3)	1.055(3)	1.042(4)	1.017(3)	1.014(3)	1.011(3)	1.009(3)	1.010(3)

[1] $w = [\sigma^2(F_\mathrm{o}) + (0.01F_\mathrm{o})^2]^{-1}$.
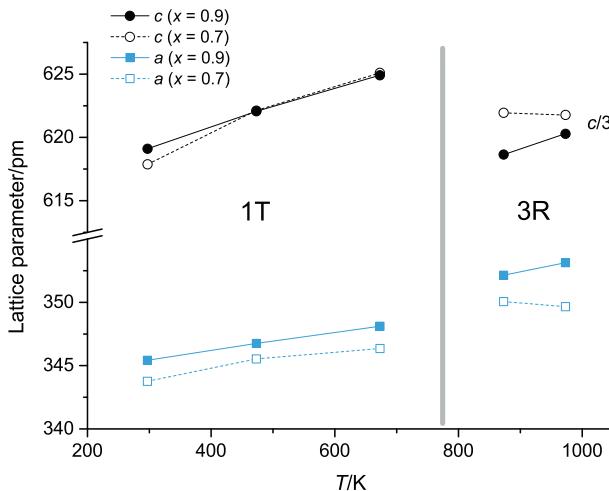[2] March–Dollase parameter for preferred orientation along (001).

Figure 3: Stacking plot of temperature-dependent diffractograms of $Li_{0.7}TiS_2$ (normalized to the intensity of the niobium (011) reflection at ca. 38.5°). 1T phase in black, 3R phase in blue/grey, container reflections cut off at high intensities for clarity.

cause of the considerable structural changes during the 1T ↔ 3R transformation, it has to be classified as reconstructive.

3.3 Evolution of lattice parameters

In the 1T regime, the lattice parameters a and c increase with temperature for both samples (see Figure 4). As expected, the difference between $x = 0.7$ and 0.9 in c is small, whereas it is considerable in a (being larger for the more lithium-rich compounds) [5, 7, 32].

In the 3R phase, these relations are reproduced for a. The lattice parameter c, however, decreases with rising lithium content. This has been explained with the differences in stacking along c (see Figure 1) using a hand-waving argument [10]: In the 1T phase, the metal ions are stacked above each other. The more lithium is inserted, the stronger is the Coloumb repulsion between them and the titanium ions of the adjacent layers – and the larger becomes c. In the 3R phase, on the other hand, the metal layers are shifted with respect to each other, so that the anion-anion repulsion dominates. The more lithium is inserted, the better is the shielding of this repulsion – and the smaller becomes c. The same argument holds for the decreasing stability of the 1T with respect to the 3R phase with increasing x at a given temperature [5].

Figure 4: Temperature evolution of the lattice parameters. a in blue/grey as squares, c in black as circles (value divided by three in the 3R regime). Li$_{0.7}$TiS$_2$ with hollow symbols and dashed lines, Li$_{0.9}$TiS$_2$ with solid symbols and lines. Lines merely guiding the eye.

To get at least semi-quantitative information, we calculated the Coloumb attraction energies using a simple ionic model. The molar lattice energy $\Delta_{latt}U_m$ is normally expressed as the sum of the molar Madelung energy $\Delta_C U_m$ (electrostatic), Born repulsion $\Delta_B U_m$, vdW attraction $\Delta_W U_m$ (dispersive), dipole-ion/dipole-dipole interactions $\Delta_{PP}U_m$ and additional smaller or corrective terms (see Eq. 1) [33]. Among these, the Madelung energy, that is easily calculated, makes up for the largest part of the attractive potential.

$$\Delta_{latt}U_m = \Delta_C U_m + \Delta_B U_m + \Delta_W U_m + \Delta_{PP}U_m + \ldots \tag{1}$$

The results are shown in Table 2. Considering only the Madelung energies, the 3R phases are more stable than the 1T phases for a given x. This finding corroborates the rationalization given in the discussion of lattice parameters above. Additionally, the stabilization is slightly larger for the lower lithium content, being probably due to less lithium-lithium repulsion. Ab-initio calculations have shown before that, for $x = 1$ at 0 K, the 1T phase is by ca. 4 kJ · mol^{-1} more stable than the 3R phase [9]. Obviously, this must be caused by covalency or other electronic effects. Interestingly, the Madelung energy is much larger for $x = 0.9$ at a given temperature (and thus in a given structure). This means that, at least in the higher-content regime, lithium intercalation is electrostatically strongly disfavored.

We analyzed the contributions to the thermodynamic properties of the two polymorphs by periodic quantum-chemical calculations. Similar to our previ-

Table 2: Madelung parts $\Delta_C U_m$/kJ $\cdot$ mol^{-1} of the molar lattice energies per unit cell for Li$_x$TiS$_2$. Effective ionic charges reduced by half.

	$x = 0.7$	$x = 0.9$	$[\Delta(\Delta_C U_m)]_T$
1T (673 K)	−2193	−2092	101
3R (873 K)	−2211	−2108	103
$[\Delta(\Delta_C U_m)]_x$	−18	−16	

Table 3: PBE relative energy ΔE/kJ $\cdot$ mol^{-1} of the 3R with respect to 1T phase for $x = 0.67$ as a function of the basis set.

Basis set[1]	Full DFT	$E_{eN} + E_{ee} + E_{NN}$
A	+23	−13
B	+9	−22
C	+10	+13

[1] See Computational Methods for details.

ous theoretical work [9], we used density-functional theory (DFT). In addition to the full-DFT total energy, the electrostatic energy computed from the Kohn-Sham wavefunction, i.e., the sum of electron-nuclear attraction E_{eN}, electron-electron repulsion E_{ee}, and nuclear repulsion E_{NN}, was computed (see Table 3).

These results have to be compared with $[\Delta(\Delta_C U_m)]_{0.7} = -18$ kJ $\cdot$ mol^{-1} from the Madelung sums in Table 2. In agreement with our previous DFT calculations, 1T is more stable than 3R. This result is independent from the BS. On the other hand, the electrostatic energy is strongly BS dependent. Only with the most accurate BS **C**, it shows the same trend as the full DFT energy. It appears that the Madelung energy corresponds to the electrostatic energy obtained with small BS which is reasonable since only point charges are considered. A full description of all polarization effects with BS **C** leads to large changes in both absolute and relative energy. It has to be noted that electron correlation also plays an important role in the phase stability. For comparison, also Hartree-Fock (HF) calculations with BS **A** were performed. The full HF energy difference, which does not contain the Coulomb part of electron correlation at all, is −15 kJ $\cdot$ mol^{-1}, being again similar to the Madelung energy. The relative electrostatic energy in this case is −13 kJ $\cdot$ mol^{-1}.

Furthermore, the evolution of the lattice parameters (see Figure 4) shows an anomalous decrease in c (by 0.3 ‰) and a (by 1.2 ‰) for 3R-Li$_{0.7}$TiS$_2$ when heating from 873 to 973 K. Although the bond distances at both temperatures are the same within the statistical error, the decreased value of the error-interval

Table 4: Refined coordinates, ADPs, bond lengths, and angles.

	1T-Li$_{0.7}$TiS$_2$			3R-Li$_{0.7}$TiS$_2$		1T-Li$_{0.9}$TiS$_2$			3R-Li$_{0.9}$TiS$_2$	
T/K	297	473	673	873	973	297	473	673	873	973
z(S1)/c	0.2371(5)	0.2339(9)	0.2328(7)	0.2568(2)	0.2568(3)	0.2346(4)	0.23417(7)	0.2354(6)	0.2556(2)	0.2561(3)
U_{11}(Ti1)/10^4 pm^2	0.0134(9)	0.0207(11)	0.0235(12)	0.0294(7)	0.0319(9)	0.0140(8)	0.0199(9)	0.0248(10)	0.0292(9)	0.0330(9)
U_{33}(Ti1)/10^4 pm^2	0.0082(13)	0.027(6)	0.027(4)	0.0393(3)	0.053(4)	0.013(2)	0.0123(3)	0.0128(18)	0.030(4)	0.027(4)
U_{eq}(Ti1)/10^4 pm^2	0.0116(7)	0.023(2)	0.0247(17)	0.0325(12)	0.0389(15)	0.0136(9)	0.0172(13)	0.0208(9)	0.0294(14)	0.0311(15)
U_{11}(Li1)/10^4 pm^2	0.0084(15)	0.029(2)	0.048(3)	0.0711(3)	0.087(4)	0.0155(12)	0.0272(15)	0.0402(19)	0.065(3)	0.076(3)
U_{33}(Li1)/10^4 pm^2	0.038(3)	0.037(7)	0.025(6)	0.0558(8)	0.068(11)	0.025(2)	0.036(4)	0.047(3)	0.063(8)	0.056(8)
U_{eq}(Li1)/10^4 pm^2	0.0183(15)	0.032(3)	0.040(3)	0.065(3)	0.080(5)	0.0185(11)	0.0301(16)	0.0425(16)	0.064(3)	0.069(3)
U_{11}(S1)/10^4 pm^2	0.0059(4)	0.0145(5)	0.0161(7)	0.0248(6)	0.0263(7)	0.0078(4)	0.0116(4)	0.0166(5)	0.0242(8)	0.0255(7)
U_{33}(S1)/10^4 pm^2	0.0366(16)	0.030(4)	0.034(3)	0.0413(3)	0.046(3)	0.0099(11)	0.019(3)	0.0330(19)	0.030(3)	0.036(4)
U_{eq}(S1)/10^4 pm^2	0.0161(6)	0.0198(13)	0.0219(12)	0.0301(10)	0.0328(12)	0.0085(4)	0.0140(9)	0.0221(7)	0.0261(11)	0.0292(13)
d(Ti1–S1)/pm^1	2.4670(18)	2.469(3)	2.473(3)	2.474(2)	2.473(3)	2.4672(14)	2.476(2)	2.491(2)	2.493(2)	2.4943(3)
d(Li1–S1)/pm^1	2.5645(19)	2.592(4)	2.606(3)	2.630(3)	2.627(3)	2.5839(15)	2.597(3)	2.603(2)	2.619(3)	2.632(3)
$\angle$(S1–Ti1–S1)/°										
– cis (6×)	88.33(6)	88.80(11)	88.90(8)	89.95(8)	89.98(9)	88.86(4)	88.91(8)	88.67(7)	89.87(8)	89.86(10)
– cis (6×)	91.67(6)	91.20(11)	91.10(8)	90.05(8)	90.02(9)	91.14(4)	91.09(8)	91.33(7)	90.13(8)	90.14(10)
– trans (3×)	180	180	180	180	180	180	180	180	180	180
$\angle$(S1–Li1–S1)/°										
– cis (6×)	84.17(5)	83.59(10)	83.31(8)	83.45(7)	83.45(8)	83.89(4)	83.77(7)	83.95(6)	84.49(7)	84.25(9)
– cis (6×)	95.83(5)	96.41(10)	96.69(8)	96.55(7)	96.55(8)	96.11(4)	96.23(7)	96.05(6)	95.51(7)	95.75(9)
– trans (3×)	180	180	180	180	180	180	180	180	180	180

[1] All six bonds are of equal length.

Table 5: Atomic positions and ADP symmetry restrictions.

		Wyckoff	x/a	y/b	z/c	U_{ij}
1T	Ti1	1a	0	0	0	$U_{22} = U_{11}, U_{12} = \frac{1}{2}U_{11}, U_{13} = U_{23} = 0$
	Li1	1b	0	0	½	$U_{22} = U_{11}, U_{12} = \frac{1}{2}U_{11}, U_{13} = U_{23} = 0$
	S1	2d	⅓	⅔	z/c	$U_{22} = U_{11}, U_{12} = \frac{1}{2}U_{11}, U_{13} = U_{23} = 0$
3R	Ti1	3a	0	0	0	$U_{22} = U_{11}, U_{12} = \frac{1}{2}U_{11}, U_{13} = U_{23} = 0$
	Li1	3b	0	0	½	$U_{22} = U_{11}, U_{12} = \frac{1}{2}U_{11}, U_{13} = U_{23} = 0$
	S1	6c	0	0	z/c	$U_{22} = U_{11}, U_{12} = \frac{1}{2}U_{11}, U_{13} = U_{23} = 0$

centre reflects the contraction of lattice parameters (see Table 4). We attribute this behaviour, that is only found for the lower lithium content and at high temperatures, to an inset of diffusion processes smoothing the lithium (charge) distribution – if enough vacancies in the lithium layer are available. The thermal evolution of the ADPs corroborates this hypothesis. Although in some cases the displacements are clearly anisotropic ($U_{11} \neq U_{33}$), we evaluated the equivalent isotropic displacement parameters U_{eq} straightforwardly. For the titanium and sulfide ions, a gradual (approximately linear) increase is found over the whole temperature range. For the lithium ions, the rise is not only steeper and starting from a somewhat higher value, but also shows an additional slope during (and for $x = 0.7$ also after) the transition to the 3R phase. This finding, which is much more pronounced for $Li_{0.7}TiS_2$, indicates an additional thermally activated dynamic process superimposed on the normal temperature evolution of ADPs and comprising only the lithium ions. A future publication will substantiate, that it is indeed lithium-ion diffusion in plane, and elaborate on this phenomenon being well beyond the scope of this work [34].

3.4 Crystal Structure of the 3R Phases

Atomic positions, structural and displacement parameters are summarized in the Tables 4 and 5. For reasons of symmetry, only two atomic displacement parameters (ADPs) per atom and one atomic coordinate overall, z(S1), can be refined.

As has been reported before for the 1T phase [7], lithium was also only found in the octahedral voids at 0, 0, ½ in 3R-$Li_x TiS_2$. Spurious negative scattering-length density occurred in tetrahedral voids, but did not significantly exceed the noise level. Test refinements did not yield positive occupations for lithium ions distributed to this site. No hint at lithium ordering was found.

The coordination environment of the titanium ion in 3R-Li$_x$TiS$_2$ is nearly perfectly octahedral, whereas the one of the lithium ion is considerably distorted. Anharmonic effects in atomic displacement were discovered that will be adequately addressed in a publication to come [34].

4 Conclusion

Powders of Li$_x$TiS$_2$ ($x = 0.7,\ 0.9$), as synthesized by us, were found to undergo a reversible reconstructive transformation from the 1T to the 3R phase when heated from 673 to 873 K. The neutron diffractograms, which we acquired at multiple temperature points, allowed for a full Rietveld refinement resulting in good to very good fits. Lithium ions were unambiguously located in octahedral voids at 0, 0, $^1/_2$ and no ordering was observed. Known trends in the temperature evolution of lattice parameters were reproduced. The hand-waiving argument explaining them was corroborated using calculations of the Madelung part of the molar lattice energy. Furthermore, we found the 3R polymorph to be electrostatically more stable than the 1T polymorph and a lithiation from $x = 0.7$ to $x = 0.9$ unfavorable. However, periodic quantum-chemical calculations indicate that this approach is oversimplified due to neglect of polarization and electron correlation effects, at least for the relative stability of the polymorphs. The anomalous decrease of lattice parameters in 3R-Li$_{0.7}$TiS$_2$, when being heated from 873 to 973 K, is tentatively attributed to effects of lithium migration.

References

1. F. Lévy (Ed.), *Intercalated Layered Materials*, D. Reidel Publishing, Dordrecht, Netherlands (1979).
2. M. S. Whittingham and A. J. Jacobson (Eds.), *Intercalation Chemistry*, Academic Press, New York, USA (1982).
3. M. S. Whittingham, Chem. Rev. **104** (2004) 4271.

4. H. A. Hallak and P. A. Lee, Solid State Commun. **47** (1983) 503.

5. K. M. Colbow, J. R. Dahn, and R. R. Haering, J. Power Sources **26** (1989) 301.

6. S. Sinha and D. W. Murphy, Solid State Ionics **20** (1986) 81.

7. J. R. Dahn, W. R. McKinnon, R. R. Haering, W. J. L. Buyers, and B. M. Powell, Can. J. Phys. **58** (1980) 207.

8. A. H. Thompson and C. R. Symon, Solid State Ionics **3–4** (1981) 175.

9. S. Nakhal, M. Lerch, J. Koopman, M. M. Islam, and T. Bredow, Z. Anorg. Allg. Chem. **639** (2013) 2822.

10. Z. Zhang, C. Dong, C. Guan, L. Yang, X. Luo, and A. Li, Mater. Res. Bull. **61** (2015) 499.

11. J. Rodríguez-Carvajal, Phys. B: Condens. Matter **192** (1993) 55.

12. M. Hoelzel, A. Senyshyn, N. Juenke, H. Boysen, W. Schmahl, and H. Fuess, Nucl. Instrum. Methods Phys. Res., Sect. A **667** (2012) 32.

13. G. Bergerhoff and I. D. Brown: Inorganic Crystal Structure Database, in: *Crystallographic Databases*, F. H. Allen, G. Bergerhoff, R. Sievers (Eds.), International Union of Crystallography, Chester, U.K. (1987), p. 77.

14. V. Petříček, M. Dušek, and L. Palatinus, Z. Kristallogr. – Cryst. Mater. **229** (2014) 345.

15. P. Thompson, D. E. Cox, and J. B. Hastings, J. Appl. Crystallogr. **20** (1987) 79.

16. J.-F. Bérar and G. Baldinozzi, J. Appl. Crystallogr. **26** (1993) 128.

17. A. March, Z. Kristallogr. Krist. **81** (1932) 285.

18. W. Dollase, J. Appl. Crystallogr. **19** (1986) 267.

19. K. Brandenburg, Diamond – Crystal and Molecular Structure Visualization, v. 3.2 (2013).

20. OriginLab, OriginPro – Data Analysis and Graphing Software, v. 9.1 (2014).

21. K. Momma and F. Izumi, J. Appl. Crystallogr. **44** (2011) 1272.

22. T. Bredow and M. Lerch, Z. Anorg. Allg. Chem. **630** (2004) 2262.

23. R. Hübenthal, M. Serafin, and R. Hoppe, MAPLE – Program for the Calculation of Distances, Angles, Effective Coordination Numbers, Coordination Spheres, and Lattice Energies, v. 4.0 (1995).

24. J. P. Perdew, K. Burke, and M. Ernzerhof, Phys. Rev. Lett. **77** (1996) 3865.

25. J. P. Perdew, K. Burke, and M. Ernzerhof, Phys. Rev. Lett. **78** (1997) 1396.

26. R. Dovesi, V. R. Saunders, C. Roetti, R. Orlando, C. M. Zicovich-Wilson, F. Pascale, B. Civalleri, K. Doll, N. M. Harrison, I. J. Bush, P. D'Arco, and M. Llunell, CRYSTAL09 – A Computational Tool for Solid State Chemistry and Physics (2009).

27. T. Bredow, P. Heitjans, and M. Wilkening, Phys. Rev. B: Condens. Matter Mater. Phys. **70** (2004) 115111.

28. M. M. Islam, T. Bredow, and C. Minot, J. Phys. Chem. B **110** (2006) 9413.

29. D. E. Woon and T. H. Dunning Jr., J. Chem. Phys. **98** (1993) 1358.

30. T. H. Dunning Jr., J. Chem. Phys. **90** (1989) 1007.

31. D. Rappoport and F. Furche, J. Chem. Phys. **133** (2010) 134105.

32. R. R. Chianelli, J. C. Scanlon, and B. M. L. Rao, J. Electrochem. Soc. **125** (1978) 1563.

33. R. Hoppe, Z. Naturforsch., A: Phys. Sci. **50** (1995) 555.

34. D. Wiedemann, M. M. Islam, S. Nakhal, A. Senyshyn, T. Bredow, and M. Lerch, submitted.